HHS Public Access

Author manuscript

ACS Nano. Author manuscript; available in PMC 2018 May 21.

Published in final edited form as:

ACS Nano. 2017 May 23; 11(5): 4916–4925. doi:10.1021/acsnano.7b01522.

Quercetin Remodels the Tumor Microenvironment To Improve the Permeation, Retention, and Antitumor Effects of Nanoparticles

Kaili Hu[†,‡], **Lei Miao**[†], **Tyler J. Goodwin**[†], **Jun Li**[†], **Qi Liu**[†], and **Leaf Huang**[†,*]

[†]Division of Pharmacoengineering and Molecular Pharmaceutics and Center for Nanotechnology in Drug Delivery, Eshelman School of Pharmacy, University of North Carolina at Chapel Hill, Chapel Hill, North Carolina 27599, United States

[‡]Murad Research Center for Modernized Chinese Medicine, Institute of Interdisciplinary Integrative Medicine Research, Shanghai University of Traditional Chinese Medicine, Shanghai 201203, People's Republic of China

Abstract

Our previous work demonstrated that Wnt16 expression in cisplatin-damaged tumor-associated fibroblasts is a key factor contributing to cisplatin resistance in malignancies. Natural antifibrotic compounds with low toxicities are promising candidates to downregulate Wnt16 expression, improving the antitumor effect of cisplatin nanoparticles. Upon screening several natural chemicals, we found that a dietary flavonoid, quercetin, significantly suppresses Wnt16 expression in activated fibroblasts. To facilitate drug delivery, we have prepared a targeted lipid/calcium/phosphate nanoparticle formulation consisting of a prodrug of quercetin, *i.e.*, quercetin phosphate, with a high loading efficiency (26.6% w/w). This quercetin nanoparticle with a particle size of around 35 nm significantly improved the bioavailability and metabolic stability of the parent quercetin. Quercetin phosphate is released from the nanoparticles and converted back to the parent quercetin under physiological conditions. Following systemic administration of quercetin phosphate nanoparticles, a significant downregulation in Wnt16 expression was observed and further yielded a synergistic antitumor effect with cisplatin nanoparticles in a stroma-rich bladder carcinoma model. The α-SMA-positive fibroblast and collagen within the tumor decreased significantly after combination treatment. This suggests that the remodeling of the tumor microenvironment induced by quercetin plays a critical role in promoting the synergy. Indeed, our data further confirmed that quercetin phosphate alone significantly remodeled the tumor microenvironment and increased the penetration of second-wave nanoparticles into the tumor nests. Collectively, quercetin phosphate nanoparticles may be a safe and effective way to improve therapeutic treatment for desmoplastic tumors.

[*]Corresponding Author: leafh@email.unc.edu.

ORCID

Leaf Huang: 0000-0002-9421-8283

Notes

The authors declare no competing financial interest.

Supporting Information

The Supporting Information is available free of charge on the ACS Publications website at DOI:10.1021/acsnano.7b01522.

Synthesis and characterization of quercetin phosphate (PDF)

Graphical Abstract

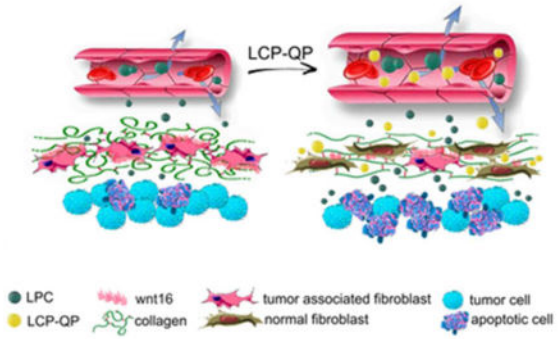

Keywords

nanoparticle; Wnt16; tumor microenvironment; cisplatin; quercetin

Stroma cells, including tumor-associated fibroblasts (TAFs), macrophage, and endothelial cells contribute to the resistance of nanochemotherapies.[1,2] These cells form a physical barrier within tumors to inhibit penetration of the therapeutic nanoparticles (NPs) as well as secrete growth-inducing cytokines and growth factors to facilitate the survival of tumor cells.[3–5] Furthermore, during the chemotherapy processes, chronic damage to stroma cells elicits the secretion of damage response program (DRP) molecules to promote the survival and growth of neighboring cells, thus causing the acquired resistance to the chemotherapies. One of these DRP molecules was reported by Sun *et al.*, who observed that treatment-induced DNA damage in the neighboring benign stroma cells promotes chemotherapy resistance through paracrine secretion of Wnt16.[6] Wnt16 is a member of the wingless-type MMTV integration site (Wnt) family considered as one of the major mitogenic growth factors that constituent DRP molecules.[7] Our previous research suggested that knockdown of Wnt16 through delivery of siRNA was an effective way to inhibit the pro-survival crosstalk between tumor cells and TAFs, ultimately suppressing tumor cell-mediated chemo-resistance.[8]

Natural chemicals have gained substantial attention in cancer therapy due to the safety profile (low toxicities). Unfortunately, the antitumor effect of natural products alone is usually far from satisfactory. There are numerous natural products with antifibrotic properties such as astragaloside IV, tetrandrine, salvianolic acid, and quercetin. However, their effect on the DRP molecule Wnt16 was unknown.[9–12] In the current study, we have screened 12 natural chemicals with reported antifibrotic activity to determine a natural inhibitor of Wnt16. Among the candidates screened, quercetin showed superior Wnt16 knockdown efficiency in NIH3T3 murine fibroblasts in the presence or absence of cisplatin. Quercetin (3,3′,4′,5,7- pentahydroxyflavone) is a naturally occurring flavonoid commonly found in fruits and vegetables. Quercetin regulates multiple biological pathways eliciting induction of apoptosis as well as inhibiting angiogenesis and proliferation.[13,14] It has also been reported to have a protective ability against oxidative stress and mutagenesisin normal cells.[15,16] However, quercetin's poor water solubility and bioavailability have limited its use as a pharmaceutical.[17,18] Quercetin was in early stage clinical trials as an anticancer agent

decades ago. Yet, due to its poor solubility, the administration required the use of solvents such as dimethyl sulfoxide or ethanol, which caused dose-dependent hemolysis as well as liver and kidney impairments.[19] Thus, alternative strategies are needed to improve the water solubility and/or the bioavailability as well as the tumor site delivery.

Phosphorylation is a commonly used method to increase the water solubility of hydrophobic drugs in prodrug development. [20,21] Therefore, we developed a quercetin prodrug through phosphorylation of the hydroxyl groups of quercetin. This modification can be cleaved *in vivo* through interaction with phosphatases. Furthermore, phosphorylation of quercetin not only increased its water solubility but also facilitated its precipitation with calcium to form an amorphous NP core used in the formulation of lipid calcium phosphate (LCP) NPs.

To improve the bioavailability and stability of quercetin, quercetin phosphate (QP) was synthesized and precipitated with calcium to be entrapped into the targeted LCP NPs. The prepared LCP-QP protects the QP from degradation and facilitates increased accumulation at the tumor site through the tumor's enhanced permeability and retention (EPR) effect. The effect of the LCP-QP as an inhibitor to the DRP molecule Wnt16 was investigated in a stroma-rich bladder carcinoma model. The effects of LCP-QP on the tumor microenvironment (TME) including TAFs apoptosis, collagen deposition, and improved NP penetration were tested. Finally, the *in vivo* toxicity of LCP-QP was inspected by biochemical indicator analysis and organ hematoxylin and eosin (H&E) stain analysis.

RESULTS

Natural Compound, Quercetin, Significantly Suppresses Wnt16 in Activated Fibroblasts

The effects of different natural chemicals on the expression of Wnt16 in activated fibroblasts NIH3T3 were detected by western-blot analysis (Figure 1A,B). The expression of Wnt16 in activated fibroblasts was inhibited to different extents by selected chemicals. Among them, chemical no. 6, quercetin showed the most significant inhibition effect with only 44% of Wnt16 expressed compared to the control group.

We next examined the Wnt16 inhibition effect of quercetin on cisplatin treated NIH3T3 cells. Consistent with previous studies, cisplatin NP induced a nearly 2-fold elevated secretion of Wnt16 in TAFs compared to untreated cells. Indeed, the cisplatin induced secretion of Wnt16 was abolished upon treatment with quercetin (Figure 1C).

Preparation and Characterization of LCP-QP

Quercetin phosphate (QP) was synthesized to improve the water solubility and facilitate the preparation of LCP-QP NPs. The chemical structure of the synthesized QP was confirmed by MS and NMRs (Figure S2 in the Supporting Information). The LC-MS results yielded an m/z of 702.88. The yellow colored QP increased water solubility compared to quercetin, and its concentration can be easily determined using a UV spectrophotometer.

The LCP-QP core and final particle were spherical and uniformly distributed under TEM (Figure 2B). The final particle has a particle size of approximately 35 nm and appears opalescence with a yellow color (Figure 2C,D). After phosphorylation, QP can be

encapsulated into LCP NPs with high encapsulation efficiency (60.8 ± 5.2%) and loading (26.6 ± 2.3%).

QP Conversion to Quercetin

To confirm that pharmacologically active quercetin is delivered to the tumor site, we first validated the conversion of QP to quercetin *in vitro* using alkaline phosphatase. After incubating QP with alkaline phosphatase for 1 h at 37 °C, quercetin was detected in the QP solution by HPLC analysis (Figure 3A). The retention time of the quercetin peak in the QP solution was identical to the quercetin standards, while the QP solution without alkaline phosphatase showed no quercetin peak. These results demonstrated that the QP was converted back to quercetin by phosphatase. We then tested this hypothesis in intact NIH3T3 cells. LCP-QP was incubated with the cells for 2 h, and following incubation, free quercetin was detected by HPLC analysis (Figure 3B). To further confirm the conversion of QP to quercetin *in vivo*, QP and LCP-QP were i.v. injected to stroma-rich UMUC3 bearing mice, and the tumors were harvested 1 h later to detect the quercetin concentration in tumor. Quercetin was detected in the tumor after both QP and LCP-QP injections with a higher accumulation of the LCP-QP (Figure 3C). Together, these results suggested that the QP delivered by LCP-QP could be converted to the active parent, quercetin, by hydrolytic enzymes extensively distributed *in vivo*.

LCP-QP Improves the Antitumor Efficacy of Cisplatin Nanoparticle (LPC) in a Stroma-Rich Xenograft Bladder Carcinoma Model

Antitumor efficacies of different treatments (LCP-QP, LPC, or LCP-QP combined with LPC) were investigated on a stroma-rich UMUC3 bladder cancer xenograft model (Figure 4). All groups were administered five injections every other day (QOD). The intravenously injected treatments consisting of LCP-QP and LPC alone showed partial tumor inhibition effects resulting in a significantly decreased tumor volume compared to the untreated group (Figure 4A). While the antitumor efficacy of the LCP-QP+LPC combination treatment elicited a significantly greater response in tumor growth inhibition compared to either the LPC or LCP-QP treatment alone, this suggests that the antitumor effect of LPC was greatly enhanced by the LCP-QP NPs. The same trend was found in tumor weight results, which suggests that LCP-QP combined with LPC treatment significantly reduced the tumor weight compared to the control, LPC-QP, and LPC groups (Figure 4B). Furthermore, compared to the LPC group, the LCP-QP+LPC group showed a reduced Wnt16 level with an increased cisplatin level in the tumor tissue, suggesting that the normalization effect of LCP-QP on Wnt16 upregulation facilitated the penetration of LPC NPs into the tumor (Figure 4C,F). After five doses of LPC treatment, the Wnt16 level in the tumors was increased 50% compared to the control group, suggesting there was a Wnt16 upregulation which correlated to tumor cell resistance. The TUNEL apoptosis assay results also illustrate the same pattern, in which the number of apoptotic cells in the LCP-QP+LPC treatment group was significantly higher than the other treatment groups, which is consistent with the tumor inhibition results (Figure 4D,E).

Nanoparticle Distribution and Tumor Microenvironment Remodeling *via* LCP-QP

We next investigated the effect of LCP-QP on the tumor microenvironment. This was tested by measuring the collagen content and α-SMA expressing fibroblast populations after various treatments. As shown in Figure 5A, all treatment groups that included the LCP-QP significantly decreased the active fibroblasts growth and amount of collagen in the tumors. Alternately, the number of active fibroblasts and collagen increased significantly after LPC treatment, while the LCP-QP treatments resulted in a 50% reduction in collagen compared to the untreated control group.

Furthermore, to understand the effect that decreased collagen content and activated fibroblast population play on subsequent NP tumor accumulation and penetration, we employed LCP containing a fluorescent probe, 1′-dioctadecyl-3,3,3′3′-tetramethylindocarbocyanine (DiI) in the LCP lipid bilayer. These LCP-DiI NPs were administered following treatment of LCP-QP to test the effect of LCP-QP on penetration of NPs in the tumor (Figure 5B). The results showed that, after three successive injections of LCP-QP, not only the total uptake of LCP-DiI by the tumor but also, more importantly, the penetration of LCP-DiI into the tumor nest (TN) were greatly enhanced. Free QP also resulted in a partial increase in the penetration of NPs into tumor cells. These findings, together with the TME remodeling results, suggest that the LCP-QP not only improves the QP delivery to the tumor site but also improves the tumor penetration of subsequent NPs administered after the LCP-QP, which may play a crucial role in the prominent antitumor effects *in vivo*.

In Vivo Toxicity of LCP-QP

An important aspect of nanotherapeutics is their safety. The body weight of the treated mice remained unchanged during the tumor inhibition experiments (Figure 6A). The serum biochemical test results showed the BUN, creatinine, AST, and ALT levels were all in the normal range, which suggests that there was no severe damage to renal and hepatic functions after LCP-QP and LCP-QP+ LPC injections (Figure 6B). Moreover, the H&E staining results also demonstrate that there was no tissue-specific toxicity to major organs (Figure 6C). These preliminary data suggest good biocompatibility and safety of the LCP-QP NPs.

DISCUSSION

Quercetin is a natural protective bioflavonoid that possesses many diverse pharmacologic activities including antioxidant, anti-inflammatory, antiproliferative, pro-apoptotic and antiangiogenic activities.[14,22,23] Quercetin has been shown to trigger multiple signal transduction pathways involving MEK/ERK, β-catenin, STAT3, EGFR/PI3K/Akt/mTOR, and Nrf2/keap1, which are associated with inflammation and carcinogenesis. [24–30] Downregulation of Wnt/β-catenin can be induced by quercetin in various types of cells, such as 4T1 mammary cancer cells and SW480 colon cancer cells.[31,32] Although quercetin has been reported to be a potent β-catenin inhibitor, its effect on the production of Wnt16 has not been observed until this current study. This report clearly demonstrates quercetin's activity in downregulating Wnt16 expression as well as in reducing tumor cells' ability to gain resistance and restructure the stroma. In addition to its effect on Wnt16, quercetin also

has a modulating effect on multiple other pathways like the mTOR, which may also contribute to the antitumor effect of LCP-QP. A detailed mechanism into the pharmacological pathway is under further investigation.[12]

Quercetin has demonstrated to reverse the oxidative stress environment, decreasing inflammation as well as inducing rearrangement of extracellular matrix (ECM) in aortic fibroblast disorders.[33] Our data exhibited the ability of LCP-QP to down regulate the α-SMA fibroblast populations and normalize the collagen content in the tumor tissue. This was consistent with the results found in human corneal fibroblasts in which quercetin is a key regulator of fibrotic markers and ECM assembly.[34] The remodeling effect of quercetin on fibroblasts may normalize the fibroblasts and the ECM which likely plays a critical role in increasing the penetration of DiI NPs into the tumor nest. Our results indicate that the LCP-QP has a better remodeling ability than free QP. This may be attributed to the enhanced delivery and stability of QP after NP encapsulation.

Due to the poor physiochemical properties of quercetin, many researchers have developed nanoformulations in an effort to increase the bioavailability of this phytochemical. Polymeric nanocapsules, nanomicelles, liposomes, and nanodiamonds as well as various other nanoformulations were employed to increase the bioavailability, protective or anticancer properties of quercetin.[19,35–37] In this paper, we describe the encapsulation of quercetin phosphate into lipid-calcium NPs as a TME modifier. Phosphorylation of quercetin into QP allows the precipitation of QP with calcium to form the particle core, which is further coated with asymmetric lipid bilayers decorated with a sigma receptor ligand aminoethylanisamide, AEAA, a tumor-specific targeting molecule. The drug loading of LCPQP is 26.6%, suggesting that one-quarter of the cargo consists of the drug. This high loading ability is attributed to the five phosphate groups on the QP as well as the supreme stability endowed by the core of the LCP particle.

The LCP-QP cargo allows for increased tumor accumulation, cellular uptake, and intracellular release of the QP. Upon delivering into cells, QP is dephosphorylated by phosphatases to release the active drug quercetin. Phosphatase exists extensively on cell membranes, cytoplasm, and lysosomes in various organs. Interestingly, subtypes of phosphatases are elevated in tumor tissues. Such phosphatases include the prostatic acid phosphatase whose level is correlated to tumor grade, the seminoma marker Regan isoenzyme of alkaline phosphatase, as well as the protein tyrosine phosphatase (PRL-3), which is upregulated in human myeloma cells and also considered as a metastasis-associated phosphatase.[38–41] Therefore, it is likely that the upregulated phosphatase in the tumor microenvironment may result in an enhanced conversion of QP to quercetin following the intratumoral delivery of LCP-QP.

Quercetin is considered to reduce the toxicity and sensitization of some potent anticancer chemicals, such as cisplatin and gemcitabine.[42–45] As a dietary polyphenolic agent, the safety profile of quercetin is well recognized.[46,47] Our preliminary toxicity studies also demonstrated good biocompatibility of QP and LCP-QP.

CONCLUSION

In this paper, a LCP-QP NP was developed to downregulate the Wnt16 levels in the TAFs and enhance the antitumor effect of LPC NPs in a stroma-rich bladder carcinoma model. The phosphorylation of quercetin results in successful construction of LCP-QP with small particle size and high drug loading. Intravenously injected LCP-QP yielded significantly enhanced antitumor efficiency in combination with potent LPC. The effect of LCP-QP on decreasing active fibroblasts and collagen content in the TME contributes to the enhanced antitumor effect of LCP-QP. The preliminary toxicity studies also showed a promising safety profile of the LCP-QP. The LCP-QP is a potential TME remodeling nanoformulation that can enhance the antitumor effects of nanotherapeutics. These results suggest that natural chemicals encapsulated into NPs may be a promising strategy to modulate TME and assist in traditional chemotherapy.

MATERIALS AND METHODS

Materials

1,2-Dioleoyl-3-trimethylammonium-propane chloride salt (DOTAP), 1,2-distearoyl-*sn*-glycero-3-phosphoethanolamine-*N*- [methoxy(polyethylene glycol)-2000] ammonium salt (DSPE-PEG2000), and dioleoylphosphatidic acid (DOPA) were purchased from Avanti Polar Lipids (Alabaster, AL). Quercetin, cholesterol, hexanol, triton X-100, and cyclohexane were provided by Sigma-Aldrich (St. Louis, MO). DSPE-PEG-AA was synthesized based on the previous reported methods.[48] Cisplatin was purchased from Acros Organics (Fair Lawn, NJ). All other chemicals were obtained from Sigma-Aldrich unless otherwise mentioned.

The mouse embryonic fibroblast cell line NIH3T3 was purchased from UNC Tissue Culture Facility. The human bladder transitional cell line UMUC3 was obtained from Dr. William Kim (University of North Carolina at Chapel Hill, NC). NIH3T3 and UMUC3 were cultured in Dulbecco's Modified Eagle's Media (Invitrogen, Carlsbad, CA), supplemented with 10% bovine calf serum (Hyclone, Logan, Utah) or 10% fetal bovine serum (Sigma, St. Louis MO), respectively, with penicillin (100 U/mL) (Invitrogen) and streptomycin (100 μg/mL) (Invitrogen).

Female athymic Balb/C nude mice 6–8 weeks of age were obtained from the University of North Carolina animal facilities. All work performed on animals was approved by the Institutional Animal Care and Use Committee at the University of North Carolina at Chapel Hill.

Screening of TCMs for Wnt16 Inhibition

Twelve antifibrotic natural chemicals selected according to the Chinese Pharmacopeia and literatures were tested for its effects on Wnt16 expression in TGF-β activated NIH3T3 cells. Specifically, NIH3T3 cells were preactivated with 10 ng/mL TGF-β. Then, the next day, the cells were treated with different chemicals at a predetermined nontoxic concentration: (1) tanshinone IIA, 4.7 μM; (2) astragaloside IV, 19 μM; (3) notoginsenoside R1, 54 μM; (4) matrine, 0.53 μM; (5) artemisinin, 160 μM; (6) quercetin, 10 μM; (7) rheinic acid, 11.43 μM;

(8) salvianolic acid B, 80 μM; (9) ligustrazine, 16 μM; (10) scutellarin, 80 μM; (11) salvianolic acid A, 20 μM; and (12) tetrandrine, 13 μM. The cells were harvested 24 h later, and western-blot assays were used to detect the expression levels of Wnt16. The chemical with the best Wnt16 inhibition effect was selected for further studies.

Effect of Quercetin on Wnt16 Expression in Cisplatin Treated NIH3T3 Cells

TGFβ activated NIH3T3 cells were treated with 10 μM free cisplatin for 3 h before being treated with 10 μM quercetin. Two days later, the cells were harvested for a western-blot assay of Wnt16 expression.

Synthesis and Characterization of Quercetin Phosphate

QP was synthesized by a method reported previously with some modification.[49] In brief, 3 mmol quercetin (1), DMAP (2.0 mmol per –OH group), and Et_3N (2.0 mmol per –OH group) were dissolved in 100 mL anhydrous THF. Then a solution of $ClP(O)(OEt)_2$ (90 mmol) in anhydrous THF (50 mL) was added dropwise under stirring in an ice–water bath over 30 min. The reaction was continued at room temperature for 24 h under nitrogen. Then the reaction mixture was diluted with EtOAc and washed with 0.5 M HCl, 5% (w/v) NaOH, brine, and water, and then dried over anhydrous Na_2SO_4. After removal of the solvent by rotary evaporation, the residue was purified using column chromatography on deactivated silica gel with petroleum ether/EtOAc (4:1–2:1) and DCM/methanol (5:1–2:1) as eluent to give the ethyl protected QP, which was characterized by HPLC-MS.

The ethyl protected QP (1.70 mmol) was dissolved in 10 mL dry dichloromethane, and 7.2 mmol trimethylsilyl bromide was added dropwise at 0 °C. After 4 h stirring, an excess of methanol was added, and the mixture stirred for 30 min. The mixture was evaporated to dryness under vacuum overnight, and the product was characterized by HPLC-MS, ^1H NMR, and ^{31}P NMR. A QP standard curve was calculated using a UV absorbance spectrum and was used to calculated QP concentrations in the LCP.

Preparation and Characterization of LCP-QP

The LCP-QP cores were prepared by water-in-oil microemulsions in an oil phase containing cyclohexane/Igepal CO-520 solution (70/30, v/v), as described previously.[50,51] Briefly, 300 μL of 30 mg/mL QP was mixed with 600 μL of 2.5 M $CaCl_2$ in 20 mL oil phase with continuous stirring. To a separate 20 mL oil phase, 600 μL of 200 mM NH_4HPO_4 was added. After 5 min, the two oil phases were mixed, 500 μL of 20 mM DOPA in chloroform was added to the emulsion, and the mixture was stirred for 30 min. Then 40 mL of absolute ethanol was added slowly. The ethanol emulsion mixture was centrifuged at 10,000 *g* for 15 min, and the precipitated LCP-QP core was collected. The precipitate was washed twice with absolute ethanol and dried under N_2. The LCP-QP cores were dissolved in 2 mL of chloroform and stored in a glass vial at −20 °C for future use.

To prepare the final LCP-QP, 11.5 mg LCP core in chloroform was mixed with 0.6 mL of 20 mM cholesterol, 0.6 mL of 20 mM DOTAP, 0.24 mL of 20 mM DSPE-PEG, and 0.06 mL of 20 mM DSPE-PEG-AA. After evaporating the chloroform, the residual lipids were suspended in water under brief sonication to form the final LCP-QP. The DiI-labeled LCP

(LCP-DiI) were prepared by the same method without addition of quercetin but with 2% DiI added to the lipids.

The particle size and zeta potential of LCP-QP were determined by a Malvern ZetaSizer Nano series (Westborough, MA). TEM images of LCP-QP cores and LCP-QP NPs (negatively stained with 2% uranyl acetate) were acquired using a JEOL 100 CX II TEM (JEOL, Japan). The drug-loading capacity and encapsulation efficiency of QP were measured using a UV spectrophotometer (D800, Beckman Coulter, Inc.). The LCPs were first lysed using a pH 4 acetic acid buffer, and the concentration was determined using a standard curve.

QP Conversion to Quercetin by Alkaline Phosphatase

The conversion of QP back to quercetin was first evaluated *in vitro* by alkaline phosphatase, a common hydrolytic enzyme. Two hundred μg of QP were mixed with 50 U of alkaline phosphatase in 1 mL OPTIZYME AP buffer and incubated at 37 °C for 1 h. The mixture was then frozen using dry ice and lyophilized. Then 400 μL acetonitrile was added to the extract and then analyzed with HPLC (Waters 600 HPLC system/717 plus autosampler) with a dual absorbance UV detector. The separation of quercetin was achieved by using a Kromasil 100-5-C18 column with methanol/acetonitrile/water 40:15:45 as the mobile phase with a flow rate of 1 mL/min at detection wavelength of 345 nm.

QP Conversion to Quercetin by NIH3T3 Cells

The conversion of QP to quercetin was further validated in live NIH3T3 cells. LCP-QP containing 200 μg QP was added to NIH3T3 cells. After 2 h incubation, the medium and cells were collected and subjected to lyophilization in 1% triton X-100. Then 400 μL acetonitrile was added, and the quercetin was detected by HPLC analysis.

QP Conversion to Quercetin *in Vivo*

Free QP and LCP-QP were i.v. injected to stroma-rich UMUC3 bearing mice at a QP dose of 30 mg/kg. One h after injection, the mice were sacrificed, and the tumors were harvested and analyzed for quercetin concentration by a UPLC-MS method. Baicalein was used as an internal standard. The homogenized tumor tissue was extracted with ethyl acetate and evaporated to dryness under nitrogen gas. After reconstituting with acetonitrile/0.1% formic acid and centrifugation, the supernatant was used for UPLC analysis. The mass spectrometer was operated in the positive ion mode with the TurboIonspray heater set at 450 °C (API3000 LC/MS/MS system, Applied Biosystems, Foster City, CA, USA). The samples were analyzed using the transition of m/z 303 → 153 amu for quercetin and m/z 271 → 123 amu for baicalein.

Antitumor Efficacy in Stroma-Rich Xenografts

The stroma-rich xenograft model was established previously.[8] UMUC3 (5×10^6) and NIH3T3 cells (2×10^6) in 100 μL of PBS were subcutaneously co-injected with Matrigel (BD Biosciences, CA) at a ratio of 1:1 (v/v) into the right flank of the mice. On the ninth day, the mice were randomly divided into four groups and subjected to the following treatments every other day: (1) control group, i.v. injection of 200 μL PBS; (2) LCP-QP

group, i.v. injection of LCP-QP corresponding to 5.5 mg/kg quercetin; (3) LPC group, i.v. injection of LPC corresponding to 1.7 mg/kg cisplatin; and (4) LCP-QP+LPC group, i.v. injection of both LCP-QP (5.5 mg/kg quercetin) and LPC (1.7 mg/kg cisplatin) on the same day. The LPC NPs were prepared as described previously.[52] These injections were given five times. Tumor volume and body weight of the mice were measured every day starting from the ninth day post-inoculation. The formula: $V = (L \times W^2)/2$ was applied to calculate tumor volume, where V is the tumor volume, L the larger perpendicular diameter, and W is the smaller perpendicular diameter. Two days after final administration, the mice were sacrificed, and the tumors were harvested and weighed. Western-blot was used to detect Wnt16 expression in the tumor tissue. ICP-MS was used to investigate the tumor accumulation of cisplatin. The tumor tissue was also washed with PBS and fixed by 4% paraformaldehyde for further studies.

TUNEL Assay

Paraffin-embedded sections of the tumor were prepared by the UNC Tissue Procurement Core. Slides were deparaffinized and rehydrated then stained using a TUNEL assay kit (Pierce) according to the manufacturer's instruction.

NP Distribution and TME Remodeling

To observe the TME remodeling effect of LCP-QP, the influence of LCP-QP on ECM markers (α-SMA and collagen) and LCP-DiI distribution was investigated.

Paraffin block sections of SRBC with different treatments were deparaffinized with xylene and a graded alcohol series. After antigen retrieval, sections were blocked with 10% goat serum and incubated with polyclonal rabbit anti-α-SMA antibody (Abcam, Cambridge, MA, USA) at 1:100 dilution overnight at 4 °C. The next day, the slides were incubated with Alexa Fluor 647 secondary antibody at a 1:100 dilution for 1 h at room temperature in the dark. Slides were rinsed with PBS and coverslipped with Vectashield containing DAPI (Vector Laboratories, Burlingame, CA, USA). Digital images were acquired *via* an Eclipse Ti–U inverted microscope (Nikon Corp., Tokyo, Japan) at 20× magnification and quantitatively analyzed on ImageJ (National Institutes of Health). Collagen content was visualized using Masson trichrome staining.

The effect of LCP-QP on LCP-DiI penetration was investigated on a GFP-3T3/UMUC3 stroma-rich tumor model. When the tumor was around 500 mm^3, the mice were i.v. administered three successive doses of LCP-blank, QP, and LCP-QP (corresponding to quercetin dose of 5.5 mg/kg). LCP-DiI was i.v. injected with the third dose of LCP-QP at a dose of 0.1 mg/kg DiI. The mice were sacrificed 24 h post-LCP-DiI injection. In order to localize and visualize the LCP-DiI penetration, the tumor was frozen and sectioned. The sections were directly stained with DAPI and observed using a Nikon light microscope (Nikon Corp., Tokyo).

Serum Biochemical Value Analysis and H&E Assay

After five doses of LCP-QP, LPC, and LCP-QP+LPC injections, blood was collected and centrifuged at 4000 rpm for 5 min to obtain the serum. Blood urea nitrogen (BUN),

creatinine, serum aspartate aminotransferase (AST), and alanine aminotransferase (ALT) levels were assayed as indicators of renal and hepatic function. Organs (heart, liver, spleen, lung, and kidney) were fixed and sectioned for H&E staining in order to evaluate the organ-specific toxicity.

Statistical Analysis

Quantitative results were expressed as mean ± SD. The analysis of variance was completed using student's *t* test and one-way analysis of variance (ANOVA). A *p* value of $p < 0.05$ was considered statistically significant.

Supplementary Material

Refer to Web version on PubMed Central for supplementary material.

Acknowledgments

This work was supported by NIH grants CA149363, CA149387, CA151652, and DK100664, the State Key Laboratory of Molecular Engineering of Polymers, Fudan University, Shanghai Rising-Star Program of China (13QA1403400), Shanghai talent development funds (201665), and Medical profession scholarship of Shanghai University of Traditional Chinese Medicine. We thank R. Watkins for the assistance in manuscript preparation.

References

1. Correia AL, Bissell MJ. The Tumor Microenvironment Is a Dominant Force in Multidrug Resistance. Drug Resist Updates. 2012; 15:39–49.
2. Meng H, Zhao Y, Dong J, Xue M, Lin YS, Ji Z, Mai WX, Zhang H, Chang CH, Brinker CJ, Zink JI, Nel AE. Two-Wave Nanotherapy to Target the Stroma and Optimize Gemcitabine Delivery to a Human Pancreatic Cancer Model in Mice. ACS Nano. 2013; 7:10048–10065. [PubMed: 24143858]
3. Gilbert LA, Hemann MT. DNA Damage-Mediated Induction of a Chemoresistant Niche. Cell. 2010; 143:355–366. [PubMed: 21029859]
4. Tredan O, Galmarini CM, Patel K, Tannock IF. Drug Resistance and the Solid Tumor Microenvironment. J Natl Cancer Inst. 2007; 99:1441–1454. [PubMed: 17895480]
5. Diop-Frimpong B, Chauhan VP, Krane S, Boucher Y, Jain RK. Losartan Inhibits Collagen I Synthesis and Improves the Distribution and Efficacy of Nanotherapeutics in Tumors. Proc Natl Acad Sci U S A. 2011; 108:2909–2914. [PubMed: 21282607]
6. Sun Y, Campisi J, Higano C, Beer TM, Porter P, Coleman I, True L, Nelson PS. Treatment-Induced Damage to the Tumor Microenvironment Promotes Prostate Cancer Therapy Resistance through Wnt16b. Nat Med. 2012; 18:1359–1368. [PubMed: 22863786]
7. Niehrs C, Acebron SP. Mitotic and Mitogenic Wnt Signalling. EMBO J. 2012; 31:2705–2713. [PubMed: 22617425]
8. Miao L, Wang Y, Lin CM, Xiong Y, Chen N, Zhang L, Kim WY, Huang L. Nanoparticle Modulation of the Tumor Microenvironment Enhances Therapeutic Efficacy of Cisplatin. J Controlled Release. 2015; 217:27–41.
9. Liu H, Wei W, Sun WY, Li X. Protective Effects of Astragaloside Iv on Porcine-Serum-Induced Hepatic Fibrosis in Rats and *in Vitro* Effects on Hepatic Stellate Cells. J Ethnopharmacol. 2009; 122:502–508. [PubMed: 19429320]
10. Hsu YC, Chiu YT, Cheng CC, Wu CF, Lin YL, Huang YT. Antifibrotic Effects of Tetrandrine on Hepatic Stellate Cells and Rats with Liver Fibrosis. J Gastroenterol Hepatol. 2007; 22:99–111. [PubMed: 17201889]
11. Liu P, Hu YY, Liu C, Zhu DY, Xue HM, Xu ZQ, Xu LM, Liu CH, Gu HT, Zhang ZQ. Clinical Observation of Salvianolic Acid B in Treatment of Liver Fibrosis in Chronic Hepatitis B. World J Gastroenterol. 2002; 8:679–685. [PubMed: 12174378]

12. Ren J, Li J, Liu X, Feng Y, Gui Y, Yang J, He W, Dai C. Quercetin Inhibits Fibroblast Activation and Kidney Fibrosis Involving the Suppression of Mammalian Target of Rapamycin and Beta-Catenin Signaling. Sci Rep. 2016; 6:23968. [PubMed: 27052477]
13. Yang CS, Landau JM, Huang MT, Newmark HL. Inhibition of Carcinogenesis by Dietary Polyphenolic Compounds. Annu Rev Nutr. 2001; 21:381–406. [PubMed: 11375442]
14. Murakami A, Ashida H, Terao J. Multitargeted Cancer Prevention by Quercetin. Cancer Lett. 2008; 269:315–325. [PubMed: 18467024]
15. Cai Q, Rahn RO, Zhang R. Dietary Flavonoids, Quercetin, Luteolin and Genistein, Reduce Oxidative DNA Damage and Lipid Peroxidation and Quench Free Radicals. Cancer Lett. 1997; 119:99–107. [PubMed: 18372528]
16. Bongiovanni GA, Soria EA, Eynard AR. Effects of the Plant Flavonoids Silymarin and Quercetin on Arsenite-Induced Oxidative Stress in Cho-K1 Cells. Food Chem Toxicol. 2007; 45:971–976. [PubMed: 17240505]
17. Wu Q, Deng S, Li L, Sun L, Yang X, Liu X, Liu L, Qian Z, Wei Y, Gong C. Biodegradable Polymeric Micelle-Encapsulated Quercetin Suppresses Tumor Growth and Metastasis in Both Transgenic Zebrafish and Mouse Models. Nanoscale. 2013; 5:12480–12493. [PubMed: 24165931]
18. Gao X, Wang B, Wei X, Men K, Zheng F, Zhou Y, Zheng Y, Gou M, Huang M, Guo G, Huang N, Qian Z, Wei Y. Anticancer Effect and Mechanism of Polymer Micelle-Encapsulated Quercetin on Ovarian Cancer. Nanoscale. 2012; 4:7021–7030. [PubMed: 23044718]
19. Yuan ZP, Chen LJ, Fan LY, Tang MH, Yang GL, Yang HS, Du XB, Wang GQ, Yao WX, Zhao QM, Ye B, Wang R, Diao P, Zhang W, Wu HB, Zhao X, Wei YQ. Liposomal Quercetin Efficiently Suppresses Growth of Solid Tumors in Murine Models. Clin Cancer Res. 2006; 12:3193–3199. [PubMed: 16707620]
20. Senter PD, Schreiber GJ, Hirschberg DL, Ashe SA, Hellstrom KE, Hellstrom I. Enhancement of the *in Vitro* and *in Vivo* Antitumor Activities of Phosphorylated Mitomycin C and Etoposide Derivatives by Monoclonal Antibody-Alkaline Phosphatase Conjugates. Cancer Res. 1989; 49:5789–5792. [PubMed: 2790791]
21. Hale JJ, Mills SG, MacCoss M, Dorn CP, Finke PE, Budhu RJ, Reamer RA, Huskey SE, Luffer-Atlas D, Dean BJ, McGowan EM, Feeney WP, Chiu SH, Cascieri MA, Chicchi GG, Kurtz MM, Sadowski S, Ber E, Tattersall FD, Rupniak NM, et al. Phosphorylated Morpholine Acetal Human Neurokinin-1 Receptor Antagonists as Water-Soluble Prodrugs. J Med Chem. 2000; 43:1234–1241. [PubMed: 10737756]
22. Feitelson MA, Arzumanyan A, Kulathinal RJ, Blain SW, Holcombe RF, Mahajna J, Marino M, Martinez-Chantar ML, Nawroth R, Sanchez-Garcia I, Sharma D, Saxena NK, Singh N, Vlachostergios PJ, Guo S, Honoki K, Fujii H, Georgakilas AG, Bilsland A, Amedei A, et al. Sustained Proliferation in Cancer: Mechanisms and Novel Therapeutic Targets. Semin Cancer Biol. 2015; 35(Suppl):S25–54. [PubMed: 25892662]
23. Russo GL. Ins and Outs of Dietary Phytochemicals in Cancer Chemoprevention. Biochem Pharmacol. 2007; 74:533–544. [PubMed: 17382300]
24. Nguyen TT, Tran E, Nguyen TH, Do PT, Huynh TH, Huynh H. The Role of Activated Mek-Erk Pathway in Quercetin-Induced Growth Inhibition and Apoptosis in A549 Lung Cancer Cells. Carcinogenesis. 2004; 25:647–659. [PubMed: 14688022]
25. Tanigawa S, Fujii M, Hou DX. Action of Nrf2 and Keap1 in Are-Mediated Nqo1 Expression by Quercetin. Free Radical Biol Med. 2007; 42:1690–1703. [PubMed: 17462537]
26. Yang Z, Liu Y, Liao J, Gong C, Sun C, Zhou X, Wei X, Zhang T, Gao Q, Ma D, Chen G. Quercetin Induces Endoplasmic Reticulum Stress to Enhance Cddp Cytotoxicity in Ovarian Cancer: Involvement of Stat3 Signaling. FEBS J. 2015; 282:1111–1125. [PubMed: 25611565]
27. Srinivasan A, Thangavel C, Liu Y, Shoyele S, Den RB, Selvakumar P, Lakshmikuttyamma A. Quercetin Regulates Beta-Catenin Signaling and Reduces the Migration of Triple Negative Breast Cancer. Mol Carcinog. 2016; 55:743–756. [PubMed: 25968914]
28. Bhat FA, Sharmila G, Balakrishnan S, Arunkumar R, Elumalai P, Suganya S, Raja Singh P, Srinivasan N, Arunakaran J. Quercetin Reverses Egf-Induced Epithelial to Mesenchymal Transition and Invasiveness in Prostate Cancer (Pc-3) Cell Line *Via* Egfr/Pi3k/Akt Pathway. J Nutr Biochem. 2014; 25:1132–1139. [PubMed: 25150162]

29. Wang K, Liu R, Li J, Mao J, Lei Y, Wu J, Zeng J, Zhang T, Wu H, Chen L, Huang C, Wei Y. Quercetin Induces Protective Autophagy in Gastric Cancer Cells: Involvement of Akt-Mtor- and Hypoxia-Induced Factor 1alpha-Mediated Signaling. Autophagy. 2011; 7:966–978. [PubMed: 21610320]

30. Siegelin MD, Reuss DE, Habel A, Rami A, von Deimling A. Quercetin Promotes Degradation of Survivin and Thereby Enhances Death-Receptor-Mediated Apoptosis in Glioma Cells. Neuro-Oncology. 2009; 11:122–131. [PubMed: 18971417]

31. Park CH, Chang JY, Hahm ER, Park S, Kim HK, Yang CH. Quercetin, a Potent Inhibitor against Beta-Catenin/Tcf Signaling in Sw480 Colon Cancer Cells. Biochem Biophys Res Commun. 2005; 328:227–234. [PubMed: 15670774]

32. Kim H, Seo EM, Sharma AR, Ganbold B, Park J, Sharma G, Kang YH, Song DK, Lee SS, Nam JS. Regulation of Wnt Signaling Activity for Growth Suppression Induced by Quercetin in 4T1Murine Mammary Cancer Cells. Int J Oncol. 2013; 43:1319–1325. [PubMed: 23900432]

33. Boumaza S, Belkebir A, Neggazi S, Sahraoui H, Berdja S, Smail L, Benazzoug Y, Kacimi G, Aouichat Bouguerra S. Therapeutic Role of Resveratrol and Quercetin on Aortic Fibroblasts of Psammomys Obesus after Oxidative Stress by Hydrogen Peroxide. Am J Ther. 2017:1.

34. McKay TB, Lyon D, Sarker-Nag A, Priyadarsini S, Asara JM, Karamichos D. Quercetin Attenuates Lactate Production and Extracellular Matrix Secretion in Keratoconus. Sci Rep. 2015; 5:9003. [PubMed: 25758533]

35. Gismondi A, Reina G, Orlanducci S, Mizzoni F, Gay S, Terranova ML, Canini A. Nanodiamonds Coupled with Plant Bioactive Metabolites: A Nanotech Approach for Cancer Therapy. Biomaterials. 2015; 38:22–35. [PubMed: 25457980]

36. El-Gogary RI, Rubio N, Wang JT, Al-Jamal WT, Bourgognon M, Kafa H, Naeem M, Klippstein R, Abbate V, Leroux F, Bals S, Van Tendeloo G, Kamel AO, Awad GA, Mortada ND, Al-Jamal KT. Polyethylene Glycol Conjugated Polymeric Nanocapsules for Targeted Delivery of Quercetin to Folate-Expressing Cancer Cells *in Vitro* and *in Vivo*. ACS Nano. 2014; 8:1384–1401. [PubMed: 24397686]

37. Zhao J, Liu J, Wei T, Ma X, Cheng Q, Huo S, Zhang C, Zhang Y, Duan X, Liang XJ. Quercetin-Loaded Nanomicelles to Circumvent Human Castration-Resistant Prostate Cancer *in Vitro* and *in Vivo*. Nanoscale. 2016; 8:5126–5138. [PubMed: 26875690]

38. Bates RJ, Chapman CM, Prout GR Jr, Lin CW. Immunohistochemical Identification of Prostatic Acid Phosphatase: Correlation of Tumor Grade with Acid Phosphatase Distribution. J Urol. 1982; 127:574–580. [PubMed: 6174741]

39. Uchida T, Shimoda T, Miyata H, Shikata T, Iino S, Suzuki H, Oda T, Hirano K, Sugiura M. Immunoperoxidase Study of Alkaline Phosphatase in Testicular Tumor. Cancer. 1981; 48:1455–1462. [PubMed: 7023658]

40. Saha S, Bardelli A, Buckhaults P, Velculescu VE, Rago C, St Croix B, Romans KE, Choti MA, Lengauer C, Kinzler KW, Vogelstein B. A Phosphatase Associated with Metastasis of Colorectal Cancer. Science. 2001; 294:1343–1346. [PubMed: 11598267]

41. Bradbury J. Metastasis in Colorectal Cancer Associated with Phosphatase Expression. Lancet. 2001; 358:1245.

42. Wang P, Henning SM, Heber D, Vadgama JV. Sensitization to Docetaxel in Prostate Cancer Cells by Green Tea and Quercetin. J Nutr Biochem. 2015; 26:408–415. [PubMed: 25655047]

43. Sliutz G, Karlseder J, Tempfer C, Orel L, Holzer G, Simon MM. Drug Resistance against Gemcitabine and Topotecan Mediated by Constitutive Hsp70 Overexpression *in Vitro*: Implication of Quercetin as Sensitiser in Chemotherapy. Br J Cancer. 1996; 74:172–177. [PubMed: 8688318]

44. Orsolic N, Car N. Quercetin and Hyperthermia Modulate Cisplatin-Induced DNA Damage in Tumor and Normal Tissues *in Vivo*. Tumor Biol. 2014; 35:6445–6454.

45. Kuhlmann MK, Horsch E, Burkhardt G, Wagner M, Kohler H. Reduction of Cisplatin Toxicity in Cultured Renal Tubular Cells by the Bioflavonoid Quercetin. Arch Toxicol. 1998; 72:536–540. [PubMed: 9765070]

46. Harwood M, Danielewska-Nikiel B, Borzelleca JF, Flamm GW, Williams GM, Lines TC. A Critical Review of the Data Related to the Safety of Quercetin and Lack of Evidence of *in Vivo*

Toxicity, Including Lack of Genotoxic/Carcinogenic Properties. Food Chem Toxicol. 2007; 45:2179–2205. [PubMed: 17698276]

47. Russo M, Spagnuolo C, Tedesco I, Bilotto S, Russo GL. The Flavonoid Quercetin in Disease Prevention and Therapy: Facts and Fancies. Biochem Pharmacol. 2012; 83:6–15. [PubMed: 21856292]
48. Banerjee R, Tyagi P, Li S, Huang L. Anisamide-Targeted Stealth Liposomes: A Potent Carrier for Targeting Doxorubicin to Human Prostate Cancer Cells. Int J Cancer. 2004; 112:693–700. [PubMed: 15382053]
49. Peng G, Du Y, Wei Y, Tang J, Peng AY, Rao L. A New Synthesis of Fully Phosphorylated Flavones as Potent Pancreatic Cholesterol Esterase Inhibitors. Org Biomol Chem. 2011; 9:2530–2534. [PubMed: 21340062]
50. Yao J, Zhang Y, Ramishetti S, Wang Y, Huang L. Turning an Antiviral into an Anticancer Drug: Nanoparticle Delivery of Acyclovir Monophosphate. J Controlled Release. 2013; 170:414–420.
51. Li J, Chen YC, Tseng YC, Mozumdar S, Huang L. Biodegradable Calcium Phosphate Nanoparticle with Lipid Coating for Systemic Sirna Delivery. J Controlled Release. 2010; 142:416–421.
52. Guo S, Wang Y, Miao L, Xu Z, Lin CM, Zhang Y, Huang L. Lipid-Coated Cisplatin Nanoparticles Induce Neighboring Effect and Exhibit Enhanced Anticancer Efficacy. ACS Nano. 2013; 7:9896–9904. [PubMed: 24083505]

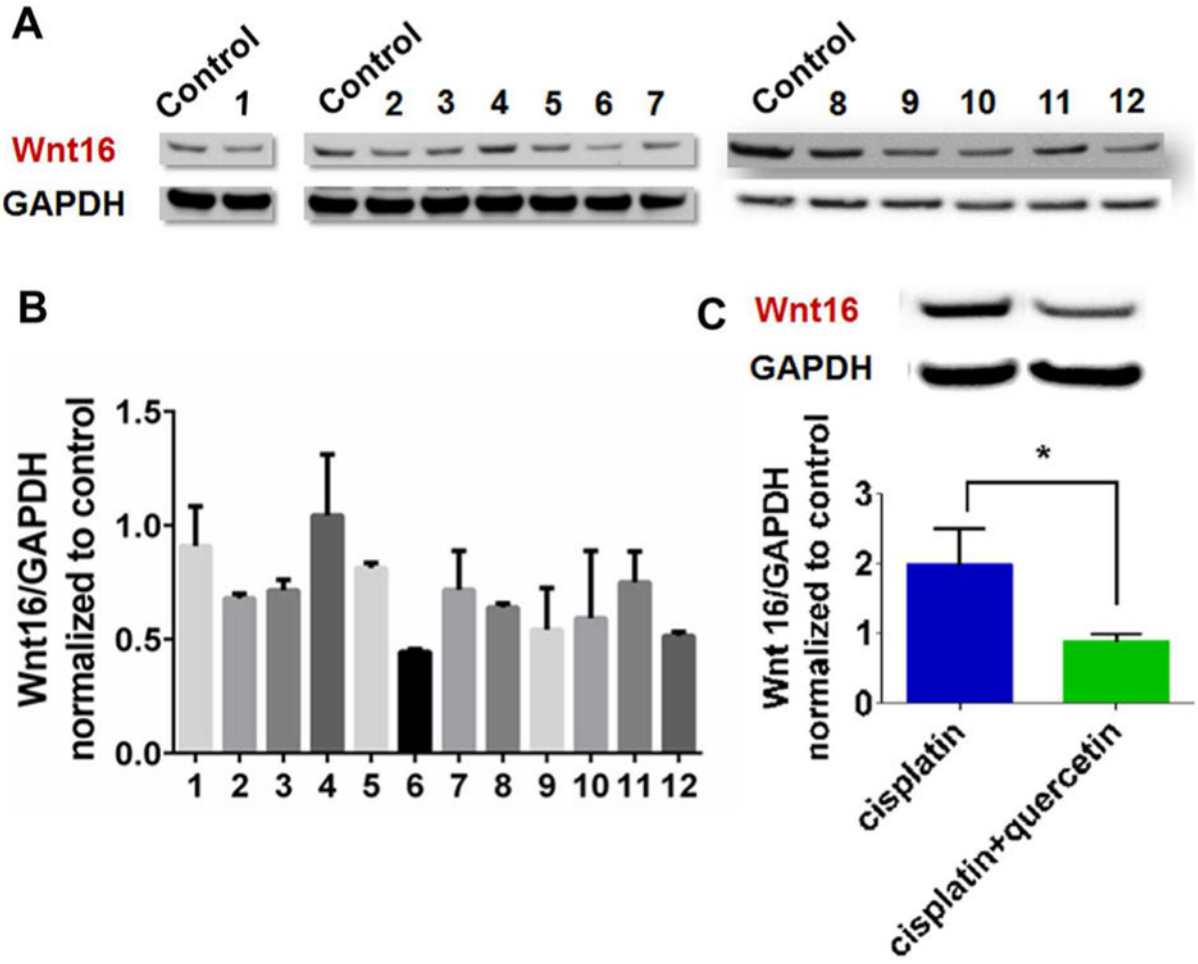

Figure 1.

Effects of selected natural chemicals on Wnt16 expression in TGF-β activated NIH3T3 cells. (A) Western-blot bands and (B) quantification of Western-blot band intensities normalized to control. (1) Tanshinone IIA, (2) astragaloside IV, (3) notoginsenoside R1, (4) matrine, (5) artemisinin, (6) quercetin, (7) rheinic acid, (8) salvianolic acid B, (9) ligustrazine, (10) scutellarin, (11) salvianolic acid A, and (12) tetrandrine. (C) Western-blot bands and quantification showed effects of quercetin on Wnt16 expression in cisplatin treated activated NIH3T3 cells. *$p < 0.05$, $n = 3$.

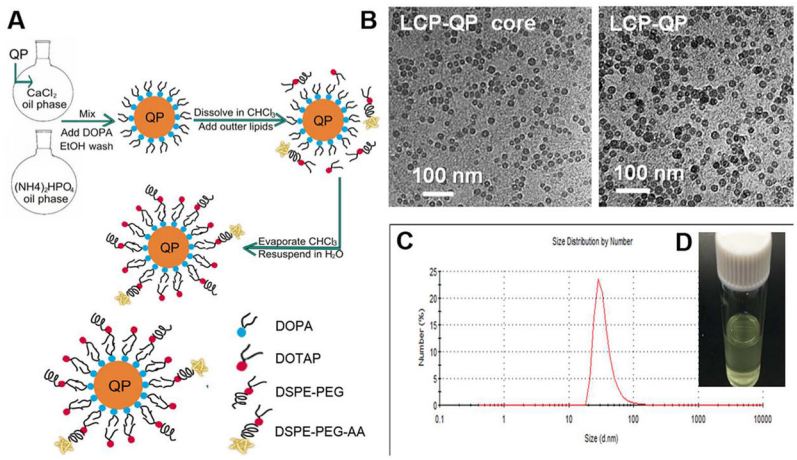

Figure 2.

Preparation and characterization of LCP-QP. (A) Preparation procedure for LCP-QP. (B) TEM photograph of LCP-QP cores and final particles. (C) Dynamic light scattering measurements of particle size and distribution of LCP-QP. (D) Photograph of LCP-QP solution.

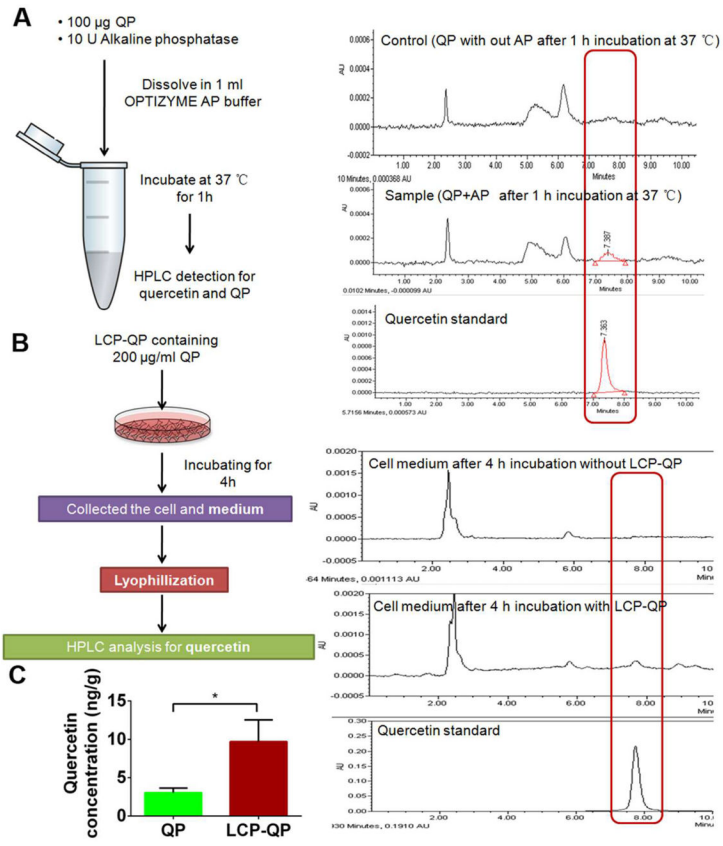

Figure 3.

QP conversion to quercetin. (A) Experiment procedure and HPLC spectrum of the solution of free QP and alkaline phosphatase after 1 h incubation at 37 °C. (B) Experiment procedure and HPLC spectrum of the cell medium after 4 h incubation of LCP-QP at 37 °C with NIH3T3 cells. (C) Tumor quercetin accumulation detected by UPLC-MS 1 h after i.v. injection of free QP and LCP-QP, respectively. $*p < 0.05$, $n = 3$.

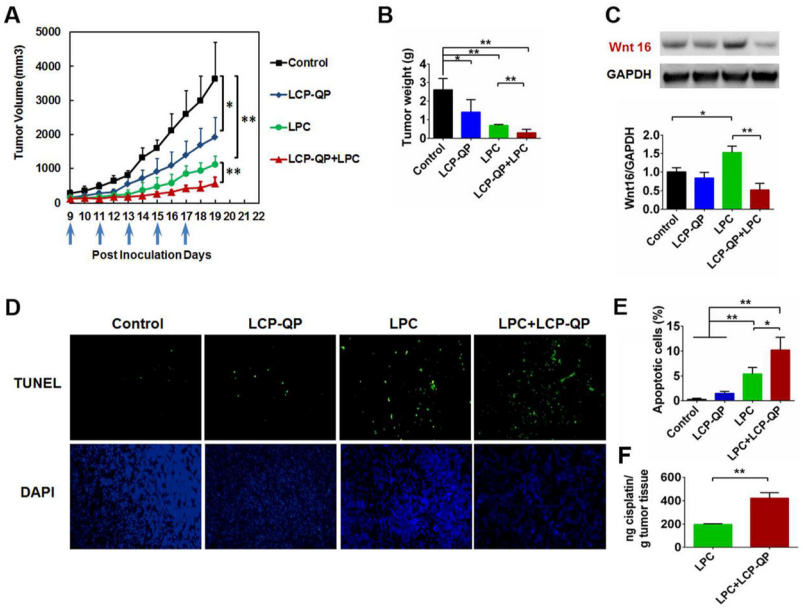

Figure 4.

Tumor inhibition effects of LCP-QP, LPC, and LCP-QP+LPC on a stroma-rich UMUC3 bladder cancer xenograft model after five i.v. injections (blue arrows, four mice per group). (A) Tumor volume change. (B) Tumor weight at the end of the experiment (day 19). (C) Western-blot bands and quantification of band intensities of Wnt16 expression in the tumor tissue after different treatments normalized to control ($n = 3$). (D) TUNEL staining of tumor sections after different treatments. (E) Quantification of TUNEL fluorescence signal expressed as the percentage of total cell number (DAPI signal). $^{**}p < 0.01$, $^{*}p < 0.05$, $n = 5$.

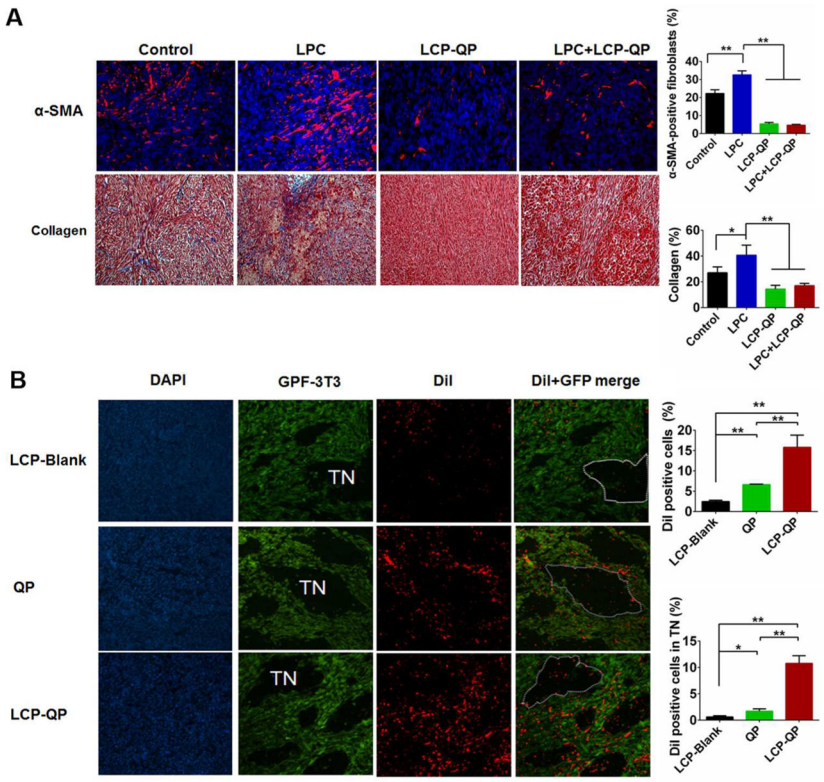

Figure 5.

(A) Effects of different treatments on the inhibition of fibroblast growth and Masson's trichrome stain for collagen and quantification results expressed as the percentage of total cell number. (B) Effect of LCP-QP on the penetration of DiI NPs and quantification of fluorescence signal (DiI labeled red) expressed as the percentage of cell number (DAPI signal) detected on frozen tumor sections. GFP positive fibroblasts (green), DAPI labeled nuclei (blue), and DiI labeled LCP-QP particles (red). $^{**}p < 0.01$, $^{*}p < 0.05$, $n = 5$.

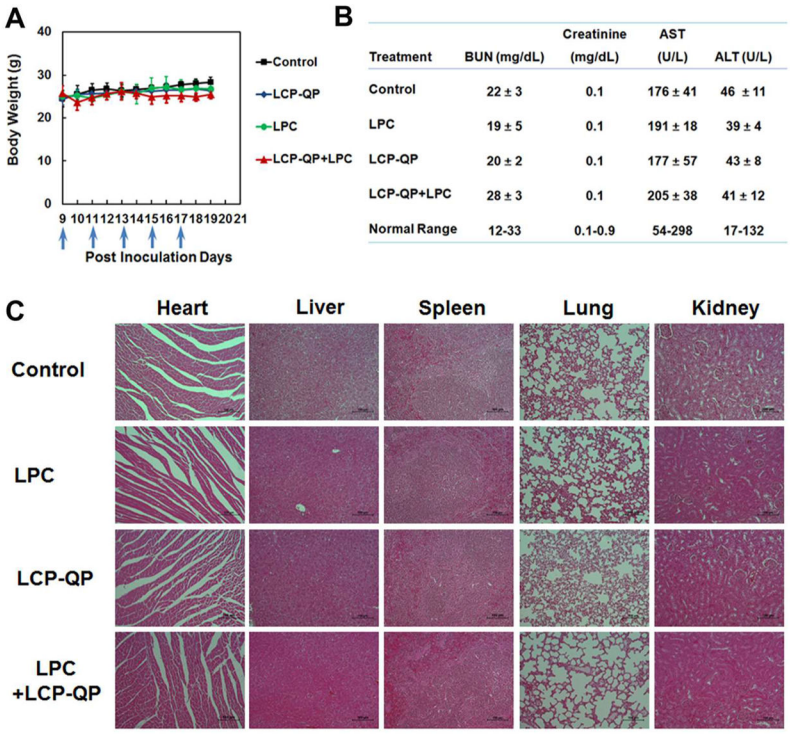

Figure 6.

(A) Body weight change. (B) Serum ALT, AST, BUN, and creatinine levels. (C) H&E staining of major drug accumulating organs after five injections of different treatments.